Journal of Biomolecular NMR (2006) 35: 89–101
DOI 10.1007/s10858-006-9006-0

Article

Molecular conformations of a disaccharide investigated using NMR spectroscopy

Clas Landersjö[a], Baltzar Stevensson[b], Robert Eklund[a], Jennie Östervall[a,b], Peter Söderman[a], Göran Widmalm[a] & Arnold Maliniak[b,*]

[a]*Arrhenius Laboratory, Department of Organic Chemistry, Stockholm University, S-106 91, Stockholm, Sweden;* [b]*Arrhenius Laboratory, Division of Physical Chemistry, Stockholm University, S-106 91, Stockholm, Sweden*

Received 19 December 2005; Accepted 10 March 2006

Key words: carbohydrates, conformation, NMR spectroscopy, residual dipolar couplings, oligosaccharides

Abstract

The molecular structure of α-L-Rha*p*-(1 → 2)-α-L-Rha*p*-OMe has been investigated using conformation sensitive NMR parameters: cross-relaxation rates, scalar $^3J_{CH}$ couplings and residual dipolar couplings obtained in a dilute liquid crystalline phase. The order matrices of the two sugar residues are different, which indicates that the molecule cannot exist in a single conformation. The conformational distribution function, $P(\phi, \psi)$, related to the two glycosidic linkage torsion angles ϕ and ψ was constructed using the APME method, valid in the low orientational order limit. The APME approach is based on the additive potential (AP) and maximum entropy (ME) models. The analyses of the trajectories generated in molecular dynamics and Langevin dynamics (LD) computer simulations gave support to the distribution functions constructed from the experimental NMR parameters. It is shown that at least two conformational regions are populated on the Ramachandran map and that these regions exhibit very different molecular order.

Abbreviations: R2R – α-L-Rha*p*-(1 → 2)-α-L-Rha*p*-OMe; RDC – residual dipolar couplings

Introduction

Determination of biomolecular structure and properties poses daunting challenges. Whereas the goal is an understanding of the biomolecular interactions and the processes that regulate different functions, one should still try to elucidate conformation and dynamics of each constituent in the system. The natural extension of these studies, namely a characterization of the interactions at atomic resolution, is presently being pursued in many laboratories. These biomolecular entities are highly complex systems in which nucleic acid–protein, protein–protein and glycoconjugates–protein interactions play major roles.

Studies of these systems in both the solid and liquid states complement each other and lead to a deepened understanding. Besides X-ray crystallography, solid-state NMR spectroscopy is a rapidly progressing technique (Castellani et al., 2002) that thereby can be used for comparison to processes taking place in solution. High resolution NMR is probably the most powerful and versatile method to gain insight into biomolecular processes ranging over many different time scales (Wang and Palmer, 2003). Information gained from NMR is of course further strengthened if additional, independent biophysical studies, such as time fluorescence depolarization, surface plasmon resonance

*To whom correspondence should be addressed.
E-mail: arnold.maliniak@physc.su.se

or isothermal titration calorimetry, can be performed on the same system.

In the field of biomolecular NMR studying nucleic acids, proteins and carbohydrates the nuclear Overhauser effect (NOE) and spin–spin couplings are well-established methods to elucidate their three-dimensional structure. The molecular dynamics (MD), on the other hand, is often characterized by employing different types of relaxation experiments. In several respects, a good description can now be obtained for a globular protein having a few hundred amino acids. However, defining the structure of carbohydrates still poses problems since usually only a limited number of NMR observables are possible to obtain between consecutive sugar residues. It is so, because severe spectral overlap, even at high magnetic fields, prevents sufficient resolution of many individual resonances. The second limitation is the fact that carbohydrates, rather than exhibiting a single well define structure, must be characterized by a distribution of conformations, which in turn requires an increased number of experimental data. During the last few years the use of dilute liquid crystalline solvents in solution-state NMR has attracted significant attention, since these systems, in addition to the classical parameters, enable determination of residual dipolar couplings (RDCs) (Tjandra and Bax, 1997a; Prestegard et al., 2000; Fung, 2002; van Buuren et al., 2004). In contrast to isotropic liquids, where the dipolar interactions are averaged to zero, the RDCs determined in liquid crystalline phases contain information on both inter-nuclear distances and orientations.

The ultimate goal in the description of the molecular structure is the determination of conformational probability distributions, which are essential for additional studies related to biomolecular interactions. In the present investigation, we analyze the conformational flexibility of the disaccharide α-L-Rha*p*-(1 → 2)-α-L-Rha*p*-OMe (R2R), shown in Figure 1, having a structural element which is found in the lipopolysaccharides anchored in the outer membrane of several pathogenic bacteria of the species *Shigella flexneri*. The conformations of the R2R molecule are determined by the two torsion angles, ϕ and ψ related to the glycosidic linkage. Using experimental NMR parameters, NOEs, *J*-couplings and RDCs, we determine the torsion angle distribution function, $P(\phi, \psi)$ for R2R. In particular we employ the APME model (Stevensson et al., 2002, 2003, Thaning et al., 2005) for construction of $P(\phi, \psi)$. The APME method, valid in the low orientational order limit, is based on the additive potential (AP) model (Emsley et al., 1982) and maximum entropy (ME) approach (Catalano et al., 1991). The APME procedure was originally demonstrated on R2R (Stevensson et al., 2002) using essentially the same experimental data set as in the present article. Here, however the analysis is substantially extended.

In addition to the experimental investigations, computer simulations of R2R in water have been carried out. In systems where hydrogen bonding occurs, it is of utmost importance that the simulations are carried out with explicit solvent molecules. Unlike α-D-Man*p*-(1 → 2)-α-D-Man*p*-(1 → *O*)-L-Ser (Lycknert et al., 2004) or cellobiose (Kroon-Batenburg et al., 1993) inter-residue hydrogen bonding is not readily accessible in R2R. Therefore, in addition to molecular dynamics (MD), we performed Langevin dynamics (LD) simulations of an isolated R2R molecule. Using LD we were able to extend the simulation length to 50 ns, which is one order of magnitude longer compared to the MD simulation. From the trajectories generated in the MD and LD simulations the torsion angle distribution functions, $P(\phi, \psi)$, were calculated and compared with experimental counterparts.

Analysis of the dipolar couplings

The through-space magnetic dipolar coupling between spins *i* and *j*, with magnetogyric ratios γ_i and γ_j, is (in Hz) given by

$$d_{ij} = -\frac{\mu_0}{8\pi^2}\frac{\gamma_i\gamma_j\hbar}{2}\left\langle (3\cos^2\theta_{ij} - 1)r_{ij}^{-3}\right\rangle \qquad (1)$$

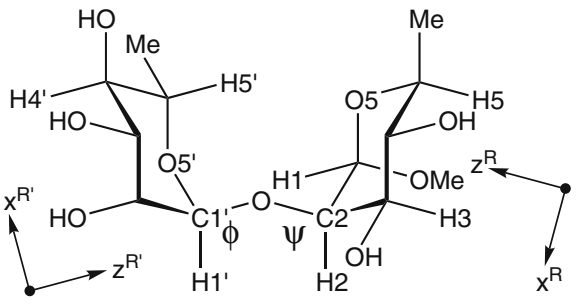

Figure 1. Schematic of the disaccharide α-L-Rha*p*-(1 → 2)-α-L-Rha*p*-OMe (R2R) in which the torsion angles at the glycosidic linkage are denoted by ϕ and ψ. Atoms in the terminal group are denoted by a prime. The local reference frames are indicated.

where θ_{ij} is the angle between the spin–spin vector and the external magnetic field, and r_{ij} is the spin–spin distance. The angular bracket denotes that the RDCs are averaged over both molecular tumbling and internal bond rotations.

For a flexible carbohydrate molecule, the observed RDCs may be expressed as

$$d_{ij} = \int d_{ij}(\Phi)P(\Phi)d\Phi \tag{2}$$

where $\Phi = \{\phi, \psi\}$ denotes a conformational state defined by the two torsion angles related to the glycosidic linkage of the disaccharide. The torsion angle probability, $P(\Phi)$, is obtained from the ensemble average over the singlet orientational distribution function (ODF) $P(\beta, \gamma, \Phi)$

$$P(\Phi) = Z^{-1} \iint P(\beta, \gamma, \Phi) \sin\beta \, d\beta \, d\gamma \tag{3}$$

where β and γ are Euler angles specifying relative orientations of molecular and director frames, and Z is a normalization factor.

In Equation 2, d_{ij} (Φ) is the RDC for a conformation with probability $P(\Phi)$. The central task in the interpretation of the RDCs is therefore to determine the torsion angle distribution function. The expression for the ODF and thus $P(\Phi)$ is derived by combining the AP model (Emsley et al., 1982) and the ME approach (Catalano et al., 1991) resulting in P_{APME} (Φ). The details of the APME procedure are outlined in the Appendix A, and the final distribution function which includes contributions from the NOEs, and J-couplings is given by

$$P_{\mathrm{APME}}(\phi, \psi) = Z''^{-1} \exp\left\{ -\sum_{ij} \lambda_{ij} d_{ij}(\phi, \psi) - \sum_{kl} \lambda_{kl} \frac{1}{r_{kl}^6(\phi, \psi)} - \sum_{mn} \lambda_{mn} {}^3J_{mn}(\phi, \psi) \right\} \tag{4}$$

where the conformational parameter Φ was replaced by the explicit torsion angles ϕ and ψ, Z'' is a normalization constant, and the conformation-dependent but orientationally averaged dipolar coupling $d_{ij}(\phi, \psi)$ is defined in Equation A.9 and Figure 2.

Using $P_{\mathrm{APME}}(\phi, \psi)$, we can calculate the averages of all the conformation dependent NMR parameters, $X(\phi, \psi)$

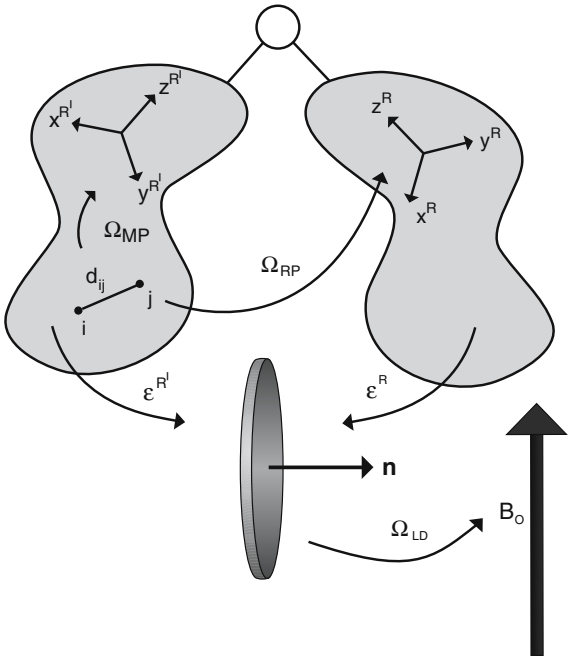

Figure 2. Required transformations in the analysis of residual dipolar couplings. The local coordinate systems are labeled x^l, y^l, z^l with $l = R, R'$ and **n** represents the director. The molecular coordinate frame (M) was arbitrarily fixed in the subunit R'.

$$\langle X \rangle = \iint X(\phi, \psi)P(\phi, \psi)d\phi \, d\psi \tag{5}$$

where $X(\phi, \psi)$ corresponds to $d_{ij}(\phi, \psi)$, $r_{kl}^{-6}(\phi, \psi)$, and ${}^3J_{mn}(\phi, \psi)$. The strategy used in the analysis is to fit the NMR parameters collected in Tables 1, 2, and 3 to Equation 5. The APME distribution function $P_{\mathrm{APME}}(\phi, \psi)$ is constructed using ε^l and λ parameters, which describe the orientational order and molecular conformations, respectively. Note that the numerical analysis must be carried out simultaneously for all adjustable parameters. This

Table 1. Averages related to the glycosidic torsion angles in R2R

	MD	LD	NMR
$<\phi>(^\circ)$	38	40	
$<\psi>(^\circ)$	−39	−33	
J_ϕ (Hz)	3.3	3.7	4.2
J_ψ (Hz)	3.9	3.6	4.8
A-state (%)	90	83	
B-state (%)	10	17	

A and *B* refer to the relative populations of the two major conformational states in the computer simulations.

Table 2. Proton–proton cross-relaxation rates and distances for R2R from 1D ^{1}H, ^{1}H T-ROESY NMR experiments and from the computer simulations[a]

Proton pair	σ (s^{-1})	r_{exp} (Å)	r_{MD} (Å)	r_{LD} (Å)
H1′–H2	0.128	2.24	2.31	2.31
H1–H5′	0.053	2.59	2.86	2.80
H1–H1′	0.018	3.10	2.92	3.07
H2–H2′	0.004	3.99	3.86	3.96
H1′–H2′	0.060	2.54[b]	2.54	2.55
H1–H2	0.058	2.55	2.52	2.53

[a]$r = \langle r^{-6} \rangle^{-1/6}$ from simulation.[b] Reference distance from MD simulation.

Table 3. Residual dipolar couplings in R2R: experimental errors in parentheses; calculated values in square parentheses

d_{CH} (Hz)		d_{HH} (Hz)[a]	
C1–H1	−17.5(0.06)[b] [−17.53][c]	H1–H3	±2.3 [+2.33]
C2–H2	−20.3(0.04) [−20.29]	H1–H5	±4.4 [−5.8]
C3–H3	+7.0(0.04) [+7.03]	H1–H6	±3.0 [−2.97]
C4–H4	+6.6(0.06) [+6.44]	H1′–H2′	+5.5/−7.4 [+7.98]
C5–H5	+4.9(0.06) [+5.09]	H1′–H3′	±1.0 [−2.04]
C1′–H1′	−15.5(0.04) [−15.51]	H1–H2′	±2.4 [+1.75][d]
C2′–H2′	−0.8(0.02) [−0.79]	H1–H3′	±1.6 [+0.07]
C3′–H3′	−13.9(0.06) [−14.44]	H2–H1′	±4.2 [−6.07]
C4′–H4′	−19.8(0.18) [−20.80]	H2–H2′	±2.2 [+1.91]
C5′–H5′	−15.6(0.06) [−14.83]	H3–H1′	±1.7 [−2.12]

[a]Estimated error for all d_{HH} is ±0.2 Hz.
[b]Standard deviation based on the jack-knife analysis procedure.
[c]Intra-residue RDCs: calculated using the order matrices.
[d]Inter-residue RDCs: calculated using the AP approach.

is because of the conformational dependence of the $\boldsymbol{\varepsilon}$ tensor, indicated in Equation A.5. The fitting was performed using a computer code written in-house, based on the MATLAB subroutine *fminu* (MATLAB v.5.0, MathWorks,1999). The fitting program minimizes the error function

$$Q = \sum_{i=1}^{N} \left(\frac{X_i^{exp} - X_i^{calc}}{s_i^{exp}} \right)^2 \quad (6)$$

where X_i^{exp} and X_i^{calc} are the experimental and calculated parameters, respectively, s_i^{exp} is the experimental standard deviation, and N is the number of measured parameters.

Materials and methods

Material

The synthesis of α-L-Rha*p*-(1 → 2)-α-L-Rha*p*-OMe (R2R) has been described previously (Norberg et al., 1986) and the ^{1}H and ^{13}C NMR assignments in D_2O have been reported (Jansson et al., 1991). For cross-relaxation NMR experiments, R2R was treated with CHELEX 100 in order to remove any paramagnetic ions. The sample was freeze-dried twice, dissolved in 0.7 ml D_2O to give a sugar concentration of 100 mM, transferred to a 5 mm NMR tube, and flame-sealed under reduced pressure after degassing by three freeze-pump-thaw cycles.

The phospholipids, 1,2-dimyristoyl-*sn*-glycero-3-phosphocholine (DMPC) and 1,2-hexanoyl-*sn*-glycero-3-phosphocholine (DHPC) were both purchased from Sigma (St. Louis, MO) and the amphiphile *N*-cetyl-*N,N,N*-trimethylammonium bromide (CTAB) was obtained from Merck (Darmstadt, Germany), all with a purity >99%. The chemicals were used without further purification.

The liquid crystalline phase was prepared from two stock solutions containing DMPC:CTAB (30:1) and DHPC in D_2O containing 20 mM phosphate buffer (pD_c = 7.1), both with a lipid concentration of 5% w/v. After sonication, the solutions were mixed to give a DMPC:DHPC molar ratio of 30:10, determined by integration of the peaks in the ^{31}P NMR spectrum at 37 °C. The sample homogeneity was ensured by several cycles of cooling (0 °C), sonication and heating (40 °C) and checked by ^{2}H NMR spectroscopy. Subsequently, 7 mg of R2R was dissolved in 0.7 ml of the liquid crystalline solvent to give a sugar concentration of 30 mM.

NMR spectroscopy

NMR experiments were performed on Varian Inova spectrometers at 14.1 and 18.8 T corresponding to ^{1}H frequencies of 600 and 800 MHz, respectively, and equipped with 5 mm PFG triple resonance probes.

Proton–proton cross-relaxation rates (σ) were obtained at 37 °C using 1D DPFGSE T-ROESY experiments (Kjellberg and Widmalm, 1999). Selective excitations of H1, H2, H1′ and H2′ in

R2R were enabled in the DPFGSE part of the pulse sequence using two 30 Hz broad i-Snob-2 shaped pulses of 57 ms duration, flanked by pulsed field gradients with durations of 1 ms and strengths of 0.8 and 2.3 G cm^{-1}, respectively. The RF field strength of the following T-ROESY spin lock was $\gamma B_1/2\pi = 3.0$ kHz.

Spectra were recorded with ten different mixing times between 30 and 800 ms, using a spectral width of 2800 Hz and 16384 complex data points. The number of transients acquired were 400–1280 with a total relaxation delay between the transients of 14.9 s, which corresponds to $> 5T_1$. Prior to Fourier transformation, the FIDs were zero-filled twice and multiplied with a 2 Hz exponential line broadening factor. Spectra were phased, drift and baseline corrected using a first-order correction and integrated using the same integration limits at all mixing times. Peak integrals of resonances due to cross-relaxation were normalized by division of the measured integrals with the extrapolated auto-peak value at zero mixing time, which was obtained after fitting the auto-peak decay to an exponential function. Proton–proton cross-relaxation build-up curves were derived from the normalized integrals at different mixing times and the rates were calculated as the initial slope by fitting these curves to a second-order polynomial. The quality of the least-square fits, expressed as the regression coefficient, was $R > 0.994$ in all cases. In addition, ^{1}H,^{1}H cross-relaxation rates were obtained for the deuterated analogue (Söderman, et al., 1998) α-L-Rha*p*-(1 → 2)-[2-^{2}H]-α-L-Rha*p*-OMe-$^2H_3$ under the same experimental conditions as described above, which showed excellent agreement with those in R2R, in particular for H1′–H1 revealing consistency in the subsequently derived inter-proton distances (data not shown). The errors in the cross-relaxation rates and the $^3J_{CH}$ values are estimated to be less than 10% and less than 0.2 Hz, respectively.

The carbon–proton residual dipolar couplings were calculated as the difference between the one-bond ^{13}C,^{1}H splitting measured at 37 °C in isotropic phase (100 mM in D_2O) and ordered phase using a slightly modified *J*-modulated HSQC experiment (Tjandra and Bax, 1997b). The couplings were obtained by fitting the cross-peak intensities from a series of experiments with different $2(T-\Delta)$ values to $C \times \cos[2\pi\, {}^1J_{CH}(T-\Delta)]$. In total, 7–10 spectra with $2(T-\Delta)$ values between 23.5 and 28 ms were recorded with spectral widths of 3000 and 10,600 Hz in F_2 and F_1, respectively. Each spectrum consisted of 4096×128 complex data points with 64–112 transients/t_1-increment, leading to an experimental time of ~8 h/experiment (isotropic phase) and ~13 h/experiment (ordered phase). Zero-filling to $16{,}384 \times 2048$ complex points, was followed by multiplication with a Gaussian weighting function prior to the Fourier transformation. Integration of the cross-peaks was performed using the same integration limits in all experiments. The quadrupolar splitting of the D_2O resonance was 10.2 Hz.

Proton–proton scalar ($^3J_{HH}$) and residual dipolar couplings (d_{HH}) were extracted from phase-sensitive COSY spectra using the NMRPipe (Delaglio et al., 1995) based fitting program Amplitude-Constrained Multiple Evaluation (ACME) (Delaglio et al., 2001). From the splittings in the spectra recorded at 37 °C, J and $J + 2d$ were obtained in the isotropic (100 mM in D_2O) and ordered phase, respectively. In all experiments a spectral width of 3000 Hz was used with $16{,}384 \times 128$ complex data points. The 160 transients/t_1-increment were acquired with a relaxation delay between the scans of $> 5T_1$, since for a quantitative analysis of the COSY cross-peaks it is important that the spin system is fully relaxed at the beginning of the pulse sequence. At the higher magnetic field strength Signed COSY experiments (Otting et al., 2000) with a ^{1}H,^{1}H TOCSY mixing time of 40 ms and a ^{1}H,^{1}H NOESY mixing time of 500 ms were performed in the ordered phase with 512 and 360 transients/t_1-increment, respectively.

Molecular simulation

Molecular dynamics and Langevin dynamics simulations used CHARMM (Brooks et al., 1983) (parallel version, C27b4) employing a CHARMM22 type of force field (MacKerell Jr. et al., 1998) modified for carbohydrates and referred to as PARM22/SU01 (Eklund and Widmalm, 2003). Initial conditions for the MD simulation were prepared by placing one R2R molecule in a previously equilibrated cubic water box of length 29.972 Å containing 900 TIP3P water molecules, and removing the solvent molecules that were closer than 2.5 Å to any solute atom. This procedure resulted in a system with R2R and 868 water molecules. Energy minimization was performed

with Steepest Descent, 1000 steps, followed by Adopted Basis Newton–Raphson until the root-mean-square gradient was less than 0.001 kcal · mol^{-1} Å^{-1}. The simulation was carried out with the leap-frog algorithm (Hockney, 1970), a dielectric constant of unity, a time step of 1 fs, and data were saved every 0.1 ps for analysis. The MD simulation was performed by heating at 5 K increments during 6 ps to 300 K, where the system was equilibrated for 100 ps, followed by the production run which lasted for 4.86 ns. The temperature was scaled by the algorithm based on a weak coupling to a thermal bath (Berendsen et al., 1984). Periodic boundary conditions and the minimum image convention were used with a non-bond frequency update every 5th step and a force shift cutoff (Steinbach and Brooks, 1994) acting to 13 Å.

In LD simulations mimicking of solute molecules in water, a collision frequency of $\gamma = 50$ ps^{-1} is often used. However, significantly increased sampling of the conformational space is possible for $\gamma = 2$ ps^{-1} (Loncharich et al., 1992) which therefore was used herein at 300 K.

Simulations were performed on an IBM SP2 computer at the Center for Parallel Computers, KTH, Stockholm, using 32 nodes, which in the MD case resulted in a CPU time of approximately 25 h per ns.

Results and discussion

In a disaccharide such as R2R, the major degrees of freedom are related to bond-rotations at the glycosidic torsion angles ϕ and ψ. The conformational distribution function for R2R was derived from the experimentally determined NMR parameters, namely: heteronuclear transglycosidic coupling constants, proton–proton cross-relaxation rates, and proton–carbon/proton–proton RDCs. In principle, these parameters can be used in the APME-analysis, Equation 4, to produce the conformational distribution function, $P_{\mathrm{APME}}(\phi,\psi)$. There is however a potential problem in the data set: we were not able, using the present experimental methods, to determine the signs of the five ^{1}H,^{1}H inter-residue RDCs. Thus, the solution is not unique, but consists of 32 (2^5) different distribution functions. We adopt, therefore, the following strategy for the analysis of the experimental data: (*i*) the conformational distribution function $P_{\mathrm{NOEJ}}(\phi,\psi)$ is determined using the cross-relaxation rates (NOEs) and scalar ($^3J_{\mathrm{CH}}$) couplings, but excluding the RDCs, (*ii*) the conformational potential function, $U_{\mathrm{int}}(\phi,\psi)$ is derived from $P_{\mathrm{NOEJ}}(\phi,\psi)$ and used together with the intra-residue dipolar couplings in the AP procedure to determine the signs of the inter-residue RDCs, and (*iii*) finally the entire data set is used in the APME procedure to derive the conformational distribution function, $P_{\mathrm{APME}}(\phi,\psi)$.

Cross-relaxation rates and scalar $^3J_{\mathrm{CH}}$ couplings

The experimental values of the scalar couplings, $^3J_{\mathrm{CH}}$, (Hardy et al., 1997) and the cross-relaxation rates from ^{1}H,^{1}H T-ROESY experiments are collected in Tables 1 and 2, respectively. Using the standard reference distance, H1′–H2′, from the molecular mechanics calculations, the other cross-relaxation rates were interpreted as effective proton–proton distances. In this interpretation, the isolated spin pair approximation (ISPA) (Keepers and James, 1984; Thomas et al., 1991) and the assumption about a single correlation time were employed. The analysis of experimental NOEs (the internuclear distances) provides important information about the molecular structure in general (Berardi et al., 1998), and in R2R in particular (Widmalm et al., 1992). The conformational distribution function, $P_{\mathrm{NOEJ}}(\phi,\psi)$, is now determined from the combination of Equations 4 and 5. Since no RDCs were employed in the analysis, only the last two terms of Equation 4 were included. Thus, the $P_{\mathrm{NOEJ}}(\phi,\psi)$ distribution function, displayed in Figure 3a, was constructed using six λ-parameters (two $^3J_{\mathrm{CH}}$, and four σ). In general, as a result of the *exo*-anomeric effect (Lemieux and Koto, 1974), it is anticipated that conformations with $\phi \sim 50^\circ$ are populated. In the $P_{\mathrm{NOEJ}}(\phi,\psi)$ distribution a single maximum is located at $\phi \sim 15^\circ$ and at $\psi \sim 0^\circ$.

Residual dipolar couplings

We now turn to the analyses of the RDCs obtained in a lyotropic liquid medium. The heteronuclear d_{CH} couplings were obtained from a series of *J*-modulated constant time HSQC experiments and homonuclear d_{HH} were derived from phase-sensitive COSY spectra. The signs of the heteronuclear RDCs were readily determined whereas for the homonuclear RDCs severe

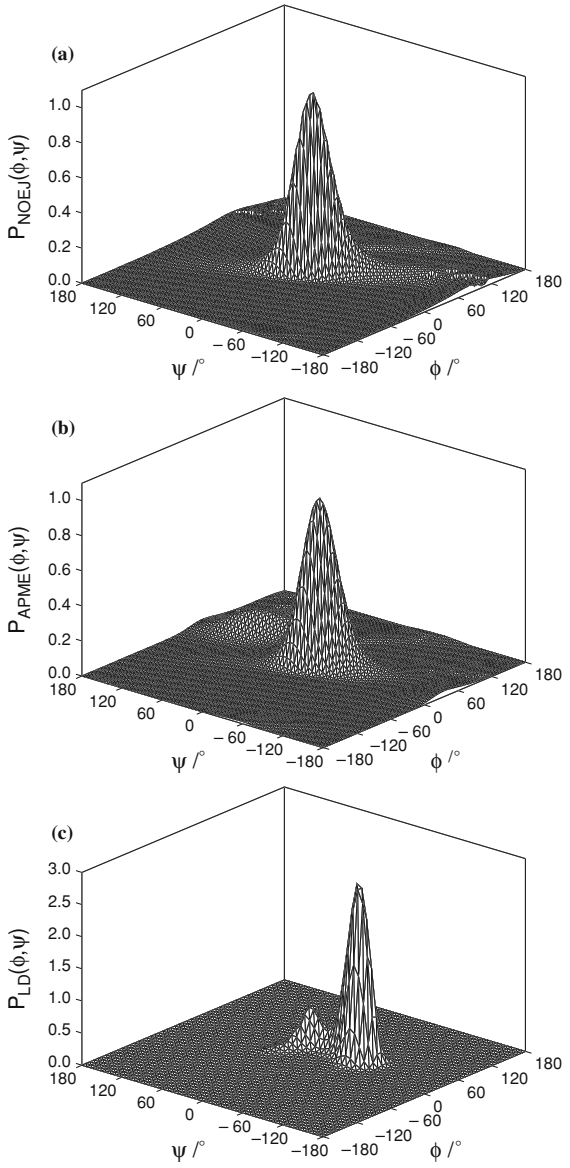

Figure 3. The conformational probability distribution for R2R: (a) derived from the analysis of the cross-relaxation and scalar $^3J_{CH}$ couplings, $P_{NOEJ}(\phi,\psi)$, (b) derived from the analysis of all experimental NMR parameters using the APME approach, $P_{APME}(\phi,\psi)$, and (c) calculated from the trajectory generated in the LD simulation, $P_{LD}(\phi,\psi)$.

difficulties were experienced, because the *J*-contribution to the splitting is absent or very small. Employing a signed-COSY experiment with TOCSY transfer we could show that the same sign was exhibited by the H4–H5, H1′–H2′, and H3′–H5′ interactions. The signed-COSY experiment with NOESY transfer revealed opposite signs between H2–H3 and H3′–H5′.

In principle, five RDCs in each residue of R2R are required for determination of the orientational order. The coordinates for all atoms in the R2R molecule, necessary for the analysis of the dipolar couplings, are collected in Table S1 (Supplementary Material). The first step in the analysis is to fix the two local frames in the rigid residues *R* and *R*′. The location of these frames is arbitrary, but we have chosen the *z* axes, z^R and $z^{R'}$, to coincide with the bonds C2–O and C1′–O in the glycosidic linkage (Figures 1 and 2). The *x* axes were located in the O–C–H planes (O–C2–H2 and O–C1′–H1′), and the *y* axes are normal to these planes. The orientations of the two local frames are provided in Table S2. The 15 intra-residual RDCs (10 heteronuclear and five homonuclear, Table 3) are then used to determine the order matrices of the rigid fragments. Diagonalisation of these matrices gives the following principal values of the order parameters: S_{zz} = 0.006251(92), $S_{xx}-S_{yy}$ = 0.003888(32) and S'_{zz} = 0.00711(19), $S'_{xx}-S'_{yy}$ = 0.008785(98) where $S_{zz} > S_{xx} > S_{yy}$ for *R* and *R*′, respectively. The principal axes of the order tensors are given in Table S3, whereas the relative orientations of the principal axes and local reference axes are included in Table S4. The order parameters S_{zz}, $S_{xx}-S_{yy}$ correspond to $\langle D^2_{0,0}\rangle$ and $\mathrm{Re}\langle D^2_{0,2}\rangle$ (Merlet et al., 1999) in the notation used in the Appendix A. Thus, the order matrices for the two residues are different and we conclude that the structure of the molecule can not be described by a single conformation. Note, that the uncertainties of the order parameters are based exclusively on the errors in the measured dipolar couplings. A distribution of the RDCs was generated from the experimental data and 10,000 randomly chosen RDC sets were used to calculate the average order tensor. We did not, however, consider the effect of the vibrational motions i.e. the uncertainty in the structure is neglected in the analysis. Furthermore, we performed a systematic rotation of the two frames related to the ordering matrix, but they were not superimposable for any single ϕ,ψ-combination. The calculated intra-residue RDCs agree well with those observed (Table 3) indicating a reasonable choice of the molecular geometry.

In the next step of the analysis we use the AP model for determination of the signs of the homonuclear inter-residue RDCs. The general drawback of the AP approach is that the functional form of the intra-molecular potential,

$U_{\text{int}}(\phi,\psi)$, must *a priori* be known. Here however, we have access to the conformational distribution function, $P_{\text{NOEJ}}(\phi,\psi)$, which, assuming the Boltzmann distribution of conformational states, gives the intra-molecular potential. Using the intra-residue RDCs and by combining Equations A3 and A4 we can determine the AP orientational distribution function $P_{\text{AP}}(\beta,\gamma,\phi,\psi)$, as given in Equation A.2. The homonuclear, inter-residue RDCs were calculated using Equation 2 and are included in Table 3. The differences between the experimental and calculated RDCs are most likely due to non-optimized intra-molecular potential function, $U_{\text{int}}(\phi,\psi)$. We have also made an attempt to analyze the RDCs using the ME approach. This analysis produced, however, an essentially flat distribution function (not shown), which is in accordance with the ME-principle (Catalano et al., 1991, Thaning et al., 2005).

The final numerical analysis was performed using the APME approach, in which 26 experimental points were used to determine 21 parameters (11 λ and 10 ε values). The values of these parameters are collected in Table 4. In the analysis, 15 intra-residue RDCs were used for determination of the ε^l parameters while the conformational parameters λ_{ij} in Equation 4 were associated with the five available trans-glycosidic RDCs. In addition, four inter-residue cross-relaxation rates related to λ_{kl} and two conformation-dependent *J*-couplings (λ_{mn}) were employed in the construction of the distribution function $P_{\text{APME}}(\phi,\psi)$ displayed in Figure 3b. This distribution function is indeed similar to $P_{\text{NOEJ}}(\phi,\psi)$ constructed from the cross-relaxation rates and scalar couplings, but excluding the RDCs. Three differences can, however, be observed: (*i*) The maximum of the $P_{\text{APME}}(\phi,\psi)$ distribution is shifted to higher ϕ-values, ($P^{\max}_{\text{NOEJ}}(\phi,\psi) \approx 14°$ and $P^{\max}_{\text{APME}}(\phi,\psi) \approx 22°$) which is in accordance with the *exo*-anomeric effect, (*ii*) $P_{\text{APME}}(\phi,\psi)$ predicts a distribution of states with positive and negative ψ-values, and (*iii*) in addition to the global maximum at $\psi \sim 0°$, $P_{\text{APME}}(\phi,\psi)$ exhibits a weak local maximum at $\psi \sim 160°$. In fact, the latter is identified as an anti-ψ conformer, which was previously observed in the Ramachandran map of the R2R molecule (Widmalm et al., 1992). Thus, we claim that including of the RDCs to the experimental data set improves the quality of the conformational distribution function.

Using this distribution and Equation 5 we calculated the averages of all the conformation dependent NMR parameters. The correlation between the calculated averages and the corresponding experimental values is displayed in Figure 4. The agreement is indeed very good which indicates reliability of the method for determination of the conformational distribution function.

Before closing this section we comment on the frequently encountered problem related to the conformational dependence of the ordering

Table 4. Parameters derived from the APME analysis of the experimental residual dipolar couplings (d), cross-relaxation rates (σ), and transglycosidic coupling constants (^3J)

$\varepsilon^l_{\alpha\beta}$		λ^p with $p = d$, σ, and ^3J	
ε^R_{zz}	0.00255	$\lambda^{^3J}_{\text{C2H1}'}$	0.515
ε^R_{xx-yy}	−0.00738	$\lambda^{^3J}_{\text{H2C1}'}$	−0.162
ε^R_{xy}	−0.00282	$\lambda^{\sigma}_{\text{H1H1}'}$	−6.30
ε^R_{xz}	−0.00173	$\lambda^{\sigma}_{\text{H1H5}'}$	−3.76
ε^R_{yz}	−0.00148	$\lambda^{\sigma}_{\text{H1H1}'}$	51.4
$\varepsilon^{R'}_{zz}$	0.000778	$\lambda^{\sigma}_{\text{H2H2}'}$	−267
$\varepsilon^{R'}_{xx-yy}$	−0.0108	$\lambda^{d}_{\text{H1H2}'}$	0.000421
$\varepsilon^{R'}_{xy}$	−0.000394	$\lambda^{d}_{\text{H1H3}'}$	0.0000163
$\varepsilon^{R'}_{xz}$	−0.00505	$\lambda^{d}_{\text{H2H1}'}$	0.163
$\varepsilon^{R'}_{yz}$	0.00221	$\lambda^{d}_{\text{H2H2}'}$	−0.200
		$\lambda^{d}_{\text{H3H1}'}$	0.426

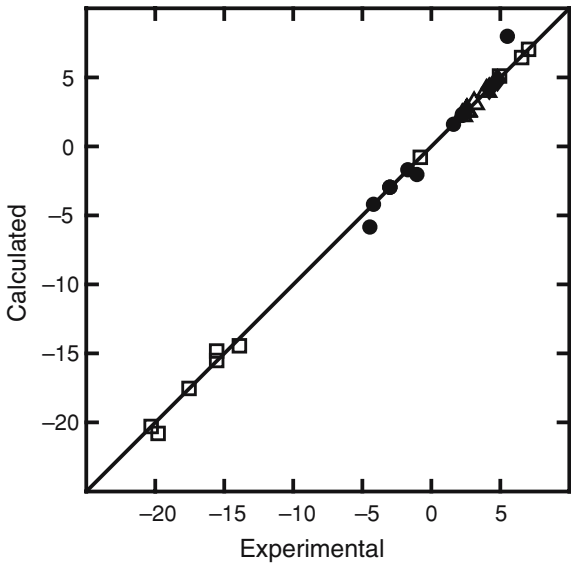

Figure 4. The correlation between observed and calculated NMR parameters from the probability distribution function for R2R: d_{CH} (squares), d_{HH} (circles), $^3J_{\text{CH}}$ (diamonds), and r_{HH} (triangles), (d_{ij} and $^3J_{mn}$ couplings in Hz; r_{kl} in Å).

(alignment) tensor. A convenient scalar parameter that characterizes the molecular ordering is the generalized degree of order (GDO), $\vartheta(\phi,\psi)$ (Prestegard et al., 2000; Tolman et al., 2001)

$$\vartheta(\phi,\psi) = \sqrt{\sum_{m=-2}^{2} \left\langle D^{2*}_{0,m}(\Omega_{DM}) \right\rangle \left\langle D^{2}_{0,m}(\Omega_{DM}) \right\rangle} \quad (7)$$

where $\left\langle D^{2}_{0,m}(\Omega_{DM}) \right\rangle$ is the orientational averaged but conformation-dependent order parameter defined in Equation A7. The advantage of the GDO concept is that it reflects both internal and orientational averaging and it can be expressed in any frame fixed in the molecule. In Figure 5 the strong conformational dependence of the GDO is demonstrated. This is further clarified in Figure 6 in which the conformational dependence of the ψ torsion angle is depicted for $\phi = 38°$ in R2R. Thus, for the conformational regions populated by R2R (cf. Figure 3) the GDO differs by up to a factor of two. Note that the averaging of $\vartheta(\phi,\psi)$ according to Equations 5 and 7 provides a single value related to the orientational order for the molecule. Using the distribution function displayed in Figure 3b the averaged GDO $\vartheta = 0.01008 \pm 0.00202$ was obtained.

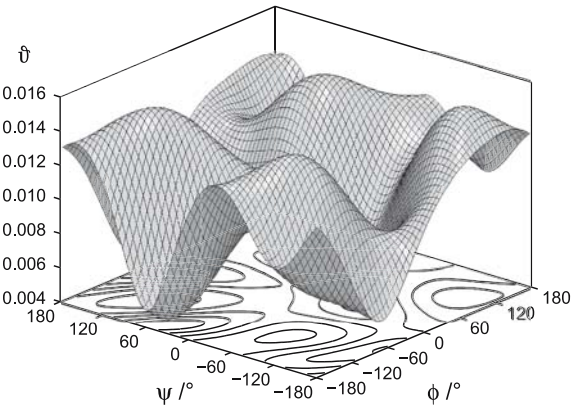

Figure 5. The conformational dependence of the generalized degree of order (GDO), $\vartheta(\phi,\psi)$.

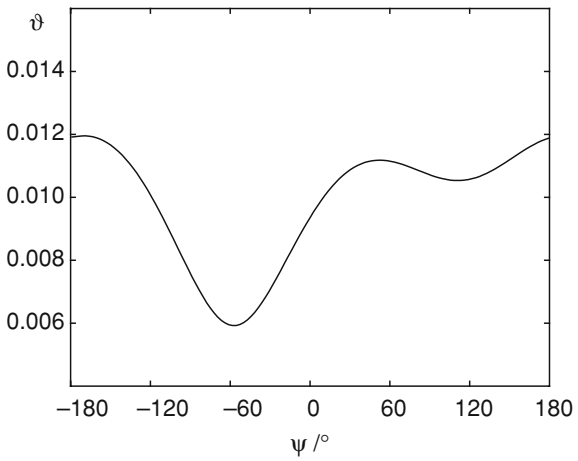

Figure 6. The conformational dependence of ϑ as a function of ψ; the slice corresponds to $\phi = 38°$.

Computer simulations

The analyses of the trajectories generated in the MD and LD computer simulations of R2R are focused on the conformational states related to the glycosidic linkage. The scatter plot of ϕ and ψ calculated from the MD trajectory is shown in Figure 7. In the plot three different conformational states can be observed: (*i*) the conformation referred to as *A* with $\psi<0°$, (*ii*) a state denoted *B* with $\psi>0°$, and (*iii*) a non-*exo*-anomeric conformation with $\phi<0°$ denoted *C*. The latter state, however, was only visited once during the MD simulation and although not completely negligible its presence is of minor importance in the present analysis. The state denoted *D*, ($\psi \sim 160°$) referred to as an anti-ψ conformer and observed in the analysis of the experimental data, is not present in

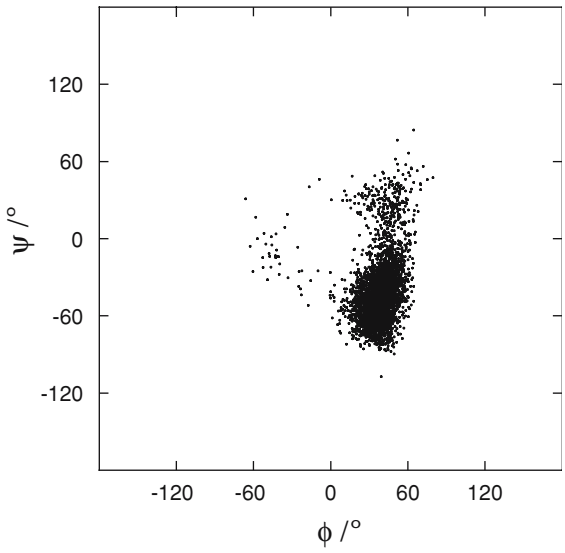

Figure 7. Scatter plot of ϕ (H1′–C1′–O2–C2) vs. ψ (C1′–O2–C2–H2) for R2R from the MD simulation.

the trajectory. Based on the LD and MD computer simulations we identify two conformational states *A* and *B* with the relative populations ~8:2 and 9:1, respectively (Table 1). Thus, also in the LD simulation the minor state is *B*.

The $^3J_{CH}$ values calculated from the trajectory using a Karplus-type relationship (Cloran et al., 1999) are given in Table 1. The experimental couplings are somewhat larger compared to those predicted by the computer simulations, indicating small discrepancies in the conformational sampling. Another possible source of error may be a deficient parameterization of the Karplus-type relationship for the $^3J_{CH}$ couplings. The average distances (Table 2), calculated from the trajectory were compared to the effective distances derived from the cross-relaxation rates measured employing ^{1}H,^{1}H T-ROESY experiments. In fact, the distances calculated from the LD simulation agree slightly better, thus indicating that the population of state *A* should be decreased compared to the MD simulation. Consequently, a significant population of the *B* state or other states is required. In Figure 3c, the conformational distribution function calculated from the LD trajectory, $P_{LD}(\phi,\psi)$ is displayed. Considering the approximations introduced in the computer simulations and in the interpretation of the experimental results, the agreement between $P_{LD}(\phi,\psi)$ and $P_{APME}(\phi,\psi)$ is indeed reasonable.

In conclusion, we have shown that it is possible to obtain the conformational distribution function, $P(\phi,\psi)$, for a small biomolecule represented here by a disaccharide. The distribution function was derived from the analysis of the conformation-dependent NMR parameters, which included residual dipolar couplings (RDCs), cross-relaxation rates and scalar *J*-couplings. The analysis involved three consecutive steps where ME approach was followed by the mean field, AP method, subsequently employing our own APME procedure. This elaborate route was chosen because at the present stage we were not able to experimentally determine the signs of the most conformation-sensitive RDCs. In the analysis we have shown that the experimental RDCs contribute to an improved conformational characterization of the molecule. Our results are of special interest due to the well known difficulty in describing conformational preferences of oligo- and polysaccharides. Furthermore, the analysis indicates a possible route for conformational investigations of more complex systems. Since there is rapid progress in the development of suitable NMR pulse sequences to allow for the determination of a large number of observables (O'Neil-Cabello et al., 2004) the methodology described here has large future potential.

Electronic supplementary material

The coordinates for all atoms in the α-L-Rha*p* (1 → 2)-α-L-Rha*p*-OMe (R2R) molecule, together with the orientations of various coordinate frames necessary for the analysis of the RDCs are given in the Supplementary Material. This material is available at http://dx.doi.org/10.1007/s10858-006-9006

Acknowledgements

This work was supported by grants from the Carl Trygger Foundation, the Swedish Research Council, the Magnus Bergvall Foundation, and SIDA/SAREC. We thank the Center for Parallel Computers, KTH, Stockholm, for putting computer facilities at our disposal and Dr. Johan Weigelt for helpful discussions. Finally, we thank a reviewer for useful comments on the analysis of the experimental data.

Appendix

APME procedure: a hybrid model based on maximum entropy and molecular field theory

The crucial step in the analysis of residual dipolar couplings (RDCs) in flexible molecules involves construction of the torsion angle distribution function for the molecular fragment under consideration. The RDC for a fixed conformational state Φ is given by

$$d_{ij}(\Phi) = b_{ij}(\Phi)\left\langle D^2_{0,0}(\Omega_{LP}(\Phi))\right\rangle = b_{ij}(\Phi)D^2_{0,0}(\Omega_{LD})\sum_{m=-2}^{2}\left\langle D^2_{0,m}(\Omega_{DM})\right\rangle D^2_{m,0}(\Omega_{MP}) \quad (A.1)$$

where the dipole–dipole coupling constant is defined as $b_{ij}(\Phi) = -\mu_0\gamma_i\gamma_j\hbar/8\pi^2 r_{ij}^3(\Phi)$ and ${}^2D_{n,m}(\Omega)$ is the second rank Wigner function (Brink and Satchler, 1993). Note that the averaging in Equation A.1 refers only to molecular orientations. Thus, the order parameters $\langle D^2_{0,m}(\Omega_{\mathrm{DM}})\rangle$ become conformation dependent via the probability distribution function $P(\beta,\gamma,\Phi)$. The transformation between the principal axis system (P) of the dipolar interaction and the laboratory frame (L) is performed explicitly using three successive rotations. Transformation between frame P and the molecular frame is characterized by Ω_{MP}, whereas the Euler angles β,γ that specify relative orientations of molecular and director frames are denoted Ω_{DM}. Finally, the orientation of the director in the magnetic field is given by Ω_{LD}. The bicelles, in the present study, orient with the normal orthogonal to the field, which results in $D^2_{0,0}(\Omega_{\mathrm{LD}}) = -1/2$. Thus in the following we will consider this rotation as a constant factor and omit it in the equations.

The additive potential (AP) model. The AP model rests on equilibrium statistical mechanics and the mean potential $U(\beta,\gamma,\Phi)$ is related to the singlet ODF by (Emsley et al., 1982)

$$P_{\mathrm{AP}}(\beta,\gamma,\Phi) = Z^{-1}\exp\{-U(\beta,\gamma,\Phi)\} \tag{A.2}$$

where $U(\beta,\gamma,\Phi)$, in units of RT, is written as the sum

$$U(\beta,\gamma,\Phi) = U_{\mathrm{int}}(\Phi) + U_{\mathrm{ext}}(\beta,\gamma,\Phi). \tag{A.3}$$

The conformational potential $U_{\mathrm{int}}(\Phi)$ is independent of molecular orientation and it is usually expressed as a cosine series. The potential of mean torque, $U_{\mathrm{ext}}(\beta,\gamma,\Phi)$, is written as

$$U_{\mathrm{ext}}(\beta,\gamma,\Phi) = -\sum_{n=-2}^{2}\varepsilon_{2,n}(\Phi)D^{2*}_{0,n}(0,\beta,\gamma) \tag{A.4}$$

where the interaction parameters $\varepsilon_{2,n}(\Phi)$ depend on the segmental, anisotropic interactions. The conformation dependence of these parameters is achieved by expressing them in terms of Φ-independent coefficients, $\varepsilon^l_{2,p}$, which represent the interactions of the lth rigid subunit with the liquid crystalline field. Thus

$$\varepsilon_{2,n}(\Phi) = \sum_l\sum_{p=-2}^{2}\varepsilon^l_{2,p}D^2_{p,n}(\Omega_{lM}) \tag{A.5}$$

where Ω_{lM} is the orientation of the lth subunit in the molecular frame.

We will now consider a situation where the orientational order is low, which in turn implies that the potential of mean torque, $U_{\mathrm{ext}}(\beta,\gamma,\Phi)$, is small. In this case, the ODF can be Taylor expanded and truncated after the second term. The analytical averaging over the molecular orientations, gives the distribution function corresponding to the low order limit of the AP model, $P'_{\mathrm{AP}}(\Phi)$ (Stevensson et al., 2002, 2003; Thaning et al., 2005)

$$\begin{aligned}P'_{\mathrm{AP}}(\Phi) &= Z'^{-1}\iint\exp\{-U_{\mathrm{int}}(\Phi)\}\\ &\quad\times[1-U_{\mathrm{ext}}(\beta,\gamma,\Phi)]\sin\beta\,d\beta\,d\gamma\\ &= Z'^{-1}\iint\exp\{-U_{\mathrm{int}}(\Phi)\}\\ &\quad\times\left[1+\sum_{n=-2}^{2}\varepsilon_{2,n}(\Phi)D^{2*}_{0,n}(0,\beta,\gamma)\right]\sin\beta\,d\beta\,d\gamma\\ &= Z'^{-1}4\pi\exp\{-U_{\mathrm{int}}(\Phi)\} = P_{\mathrm{iso}}(\Phi)\end{aligned} \tag{A.6}$$

where $P_{\mathrm{iso}}(\Phi)$ is related to the internal potential $U_{\mathrm{int}}(\Phi)$, and Z', $Z'/4\pi$ are the normalization constants for $P'_{\mathrm{AP}}(\Phi)$ and $P_{\mathrm{iso}}(\Phi)$, respectively. Thus, for a weakly ordered system, $P'_{\mathrm{AP}}(\Phi) = P_{\mathrm{iso}}(\Phi)$. The integral over the second term in Equation A.6 vanishes for all n due to properties of the Wigner functions (Brink and Satchler, 1993). Using the low order approximation and Equation A.4, we can express the conformation-dependent order parameters

$$\begin{aligned}\left\langle D^2_{0,m}(\Omega_{\mathrm{DM}})\right\rangle &\approx Q(\Phi)^{-1}\iint\exp\{-U_{\mathrm{int}}(\Phi)\}\\ &\quad\times[1-U_{\mathrm{ext}}(\beta,\gamma,\Phi)]D^2_{0,m}(0,\beta,\gamma)\sin\beta\,d\beta\,d\gamma\\ &= \frac{1}{4\pi}\iint\left[D^2_{0,m}(0,\beta,\gamma)+\sum_{n=-2}^{2}\varepsilon_{2,n}(\Phi)\right.\\ &\quad\left.\times D^{2*}_{0,n}(0,\beta,\gamma)D^2_{0,m}(0,\beta,\gamma)\right]\sin\beta\,d\beta\,d\gamma\\ &= \frac{1}{4\pi}\left[0+\sum_{n=-2}^{2}\varepsilon_{2,n}(\Phi)\frac{4\pi\delta_{n,m}}{5}\right] = \frac{\varepsilon_{2,m}(\Phi)}{5}.\end{aligned} \tag{A.7}$$

The Kronecker delta $\delta_{n,m}$ is a consequence of the orthogonality of the Wigner functions (Brink and Satchler, 1993), and $Q(\Phi) = 4\pi\exp\{-U_{\mathrm{int}}(\Phi)\}$ is the conformation dependent partition function.

The R2R disaccharide consists of two rigid subunits R and R', in which the coordinate frames are fixed with a relative orientation given by $\Omega_{RR'}$. The molecular coordinate frame (M) can be arbitrarily chosen to coincide with one of these rigid subunits. Using Equations A1, A5, and A7, we can define a conformation-dependent but orientationally averaged RDC

$$d_{ij}(\Phi) = \frac{b_{ij}(\Phi)}{5} \sum_{m=-2}^{2} \left[\varepsilon_{2,m}^{M} + \sum_{n=-2}^{2} \varepsilon_{2,n}^{R} D_{n,m}^{2}(\Omega_{RM}) \right] \times D_{m,0}^{2}(\Omega_{\mathrm{MP}}) \tag{A.8}$$

where the molecular frame was arbitrarily fixed in the subunit R'. Using the closure properties of the Wigner functions (Brink and Satchler, 1993), Equation A.8 can be simplified to

$$d_{ij}(\Phi) = \frac{b_{ij}(\Phi)}{5} \sum_{m=-2}^{2} \varepsilon_{2,m}^{M} D_{m,0}^{2}(\Omega_{\mathrm{MP}}) + \varepsilon_{2,m}^{R} D_{m,0}^{2}(\Omega_{\mathrm{RP}}). \tag{A.9}$$

In Figure 2 we show the location of the various frames relevant for the analyses of the RDCs.

Combination of the AP and ME approaches: the APME model. Assuming low orientational order, the conformational distribution function $P'_{\mathrm{AP}}(\Phi)$ was related, in Equation A.6, to the internal potential $U_{\mathrm{int}}(\Phi)$. The conformational distribution function for the glycosidic linkage in R2R depends on the torsion angles ϕ and ψ. The choice of the functional form for the potential functions for these angles is not obvious. The least biased approach that requires minimum a priori information is the ME method (Catalano et al., 1991). We therefore use the ME approach to describe the conformational dependence of the RDCs. In addition, the functional form of the ME method facilitates inclusion of the conventional NMR parameters (NOEs and J-couplings) used in present study for structure determination. Combination of the low orientational order approximation of the AP model with the ME distribution function yields the APME distribution function (Stevensson et al., 2003) given in Equation 4.

References

Berardi, R., Spinozzi, F. and Zannoni, C. (1998) *J. Chem. Phys.* **109**, 3742–3759.

Berendsen, H.J.C., Postma, J.P.M., van Gunsteren, W.F., DiNola, A. and Haak, J.R. (1984) *J. Chem. Phys.* **81**, 3684–3690.

Brink, D.M. and Satchler, G.R. (1993) *Angular Momentum* Clarendon Press, Oxford.

Brooks, B.R., Bruccoleri, R.E., Olafson, B.D., States, D.J., Swaminathan, S. and Karplus, M. (1983) *J. Comput. Chem.* **4**, 187–217.

Castellani, F., van Rossum, B., Diehl, A., Schubert, M., Rehbein, K. and Oschkinat, H. (2002) *Nature* **420**, 98–102.

Catalano, D., Di Bari, L., Veracini, C.A., Shilstone, G.N. and Zannoni, C. (1991) *J. Chem. Phys.* **94**, 3928–3935.

Cloran, F., Carmichael, I. and Serianni, A.S. (1999) *J. Am. Chem. Soc.* **121**, 9843–9851.

Delaglio, F., Grzesiek, S., Vuister, G.W., Zhu, G., Pfeifer, J. and Bax, A. (1995) *J. Biomol. NMR* **6**, 277–293.

Delaglio, F., Wu, Z. and Bax, A. (2001) *J. Magn. Reson.* **149**, 276–281.

Eklund, R. and Widmalm, G. (2003) *Carbohydr. Res.* **338**, 393–398.

Emsley, J.W., Luckhurst, G.R. and Stockley, C.P. (1982) *Proc. R. Soc. Lond. A* **381**, 117–138.

Fung, B.M. (2002) *Prog. Nucl. Magn. Reson. Spectrosc.* **41**, 171–186.

Hardy, B.J., Bystricky, S., Kovac, P. and Widmalm, G. (1997) *Biopolymers* **41**, 83–96.

Hockney, R.W. (1970) *Meth. Comput. Phys.* **9**, 136–211.

Jansson, P.-E., Kenne, L. and Widmalm, G. (1991) *Acta Chem. Scand.* **45**, 517–522.

Keepers, J.W. and James, T.L.J. (1984) *Magn. Reson.* **57**, 404–426.

Kjellberg, A. and Widmalm, G. (1999) *Biopolymers* **50**, 391–399.

Kroon-Batenburg, L.M.J., Kroon, J., Leeflang, B.R. and Vliegenthart, J.F.G. (1993) *Carbohydr. Res.* **245**, 21–42.

Lemieux, R.U. and Koto, S. (1974) *Tetrahedron* **30**, 1933–1944.

Loncharich, R.J., Brooks, B.R. and Pastor, R.W. (1992) *Biopolymers* **32**, 523–535.

Lycknert, K., Helander, A., Oscarson, S., Kenne, L and Widmalm, G. (2004) *Carbohydr. Res.* **339**, 1331–1338.

MacKerell, Jr. A.D., Bashford, D., Bellott, M., Dunbrack, Jr. R.L., Evanseck, J.D., Field, M.J., Fischer, S., Gao, J., Guo, H., Ha, S., Joseph-McCarthy, D., Kushnir, L., Kuczera, K., Lau, F.T.K., Mattos, C., Michnick, S., Ngo, T., Nguyen, T.D., Prodhom, B., Reiher, III W.E., Roux, B., Schlenkrich, M., Smith, J.C., Stote, R., Straub, J., Watanabe, M., Wiórkiewicz-Kuczera, J., Yin, D. and Karplus, M. (1998) *J. Phys. Chem. B* **102**, 3586–3616.

Merlet, D., Emsley, J.W., Lesot, P. and Courtieu, J. (1999) *J. Chem. Phys.* **111**, 6890–6896.

Norberg, T., Oscarson, S. and Szönyi, M. (1986) *Carbohydr. Res.* **156**, 214–217.

O'Neil-Cabello, E., Bryce, D.L., Nikonowicz, E.P. and Bax, A. (2004) *J. Am. Chem. Soc.* **126**, 66–67.

Otting, G., Rückert, M., Levitt, M.H. and Moshref, A. (2000) *J. Biomol. NMR* **16**, 343–346.

Prestegard, J.H., Al-Hashimi, H.M. and Tolman, H.M. (2000) *Quart. Rev. Biophys.* **33**, 371–424.

Steinbach, P.J. and Brooks, B.R. (1994) *J. Comput. Chem.* **15**, 667–683.
Stevensson, B., Landersjö, C., Widmalm, G. and Maliniak, A. (2002) *J. Am. Chem. Soc.* **124**, 5946–5947.
Stevensson, B., Sandström, D. and Maliniak, A. (2003) *J. Chem. Phys.* **119**, 2738–2746.
Söderman, P., Oscarson, S. and Widmalm, G. (1998) *Carbohydr. Res.* **312**, 233–237.
Thaning, J., Stevensson, B. and Maliniak, A. (2005) *J. Chem. Phys.* **123**, 044507-1-6.
Thomas, P.D., Basus, V.J. and James, T.L. (1991) *Proc. Natl. Acad. Sci. USA* **88**, 1237–1241.
Tjandra, N. and Bax, A. (1997a) *J. Magn. Reson.* **124**, 512–515.
Tjandra, N. and Bax, A. (1997b) *Science* **278**, 1111–1114.
Tolman, J.R., Al-Hashimi, H.M., Kay, L.E. and Prestegard, J.H. (2001) *J. Am. Chem. Soc.* **123**, 1416–1424.
van Buuren, B.N.M., Schleucher, J., Wittmann, V., Griesinger, C., Schwalbe, H. and Wijmenga, S.S. (2004) *Angew. Chem. Int. Ed.* **43**, 187–192.
Wang, C., Arthur, G. and Palmer, III A.G. (2003) *Magn. Reson. Chem.* **41**, 866–876.
Widmalm, G., Byrd, R.A. and Egan, W. (1992) *Carbohydr. Res.* **229**, 195–211.